Journal of the Serbian Chemical Society
JSCS-info@shd.org.rs • www.shd.org.rs/JSCS
J. Serb. Chem. Soc. 79 (7) S87–S94 (2014)
Supplementary material

SUPPLEMENTARY MATERIAL TO

An experimental and computational investigation of the effects of temperature on soot formation mechanisms

XIAOJIE BI[1,2], MAOYU XIAO[1], XINQI QIAO[1], CHIA-FON F. LEE[2,3] and YU LIU[4]*

[1]Key Laboratory for Power Machinery and Engineering of the Ministry of Education, Shanghai Jiao Tong University, Shanghai, 200240, China, [2]Department of Mechanical Science and Engineering, University of Illinois at Urbana-Champaign, IL, 61801, USA, [3]Center for Combustion Energy and State Key Laboratory of Automotive Safety and Energy, Tsinghua University, Beijing 100084, China and [4]Key Laboratory of Automobile Dynamic Simulation, Jilin University, Changchun, Jilin, 130012, China

J. Serb. Chem. Soc. 79 (7) (2014) 881–895

DETAILS OF THE APPARATUS

At the center of the chamber head, a hydraulic-actuated electronic-controlled unit injector (HEUI, Caterpillar) was mounted, the relevant configurations of which are given in Table S-I. In order to mimic realistic diesel engine operation conditions, the cylinder wall was heated to 380 K by eight heaters made of Watlow Firerod and the temperature of the oil line and fuel line inside the chamber head were kept at 350 K. The in-cylinder pressure was measured by a quartz pressure transducer (Kistler 6121) embedded in the chamber wall in conjunction with a charge amplifier.

TABLE S-I. Configuration of the HEUI 300A injector and the fuel injection conditions

Parameter	Value
Nozzle style	Valve covered orifice
Number of nozzle holes	6
Spray angle	140°
Orifice diameter	0.145 mm
Injection pressure	134 MPa
Injection duration	3.5 ms
Fuel volume	120 mm^3
Fuel temperature	350 K

As shown in Fig. 1, images were obtained using a high-speed digital camera (Phantom V7.1) above the optical chamber and a light source was provided by a copper vapor laser (Oxford Lasers LS20-50). Two-wavelength output at 511 and 578 nm with a power ratio of 2:1was provided by a copper-vapor laser. The high-speed camera and the copper-vapor laser were set

---

* Corresponding author. E-mail: xiaojie2163@hotmail.com

to be synchronized up to 15037 frames per second to provide time related records at a resolution of 256×256 pixels. Only one of the six spray jets was examined in the experiment. A 105 mm focal length lens made by Nikkor with a maximum aperture of *f* 4.5 was adopted for the images taking. To suppress flame emission, two interference filters at 510 and 515 nm with 10 nm full width at half maximum (FWHM) were adopted to filter out the light at 578 nm. A FWHM of 5 nm could be achieved when these two filters were aligned together. Before laser light entrance into the test constant volume chamber, it was focused by a condenser through a 6 mm diameter reflecting mirror in front of the condenser lens to a point source. The high-speed camera was triggered by injection signal and was set to record the whole combustion process of diesel fuel.

MEASUREMENTS AND SUBSEQUENT CALCULATION OF THE EXTINCTIONS

As shown in Fig. S-1, the laser beam passed through the soot cloud twice in the forward illumination technique. Therefore, the light intensity should be adjusted by the extinction due to light diffuser and soot absorption.

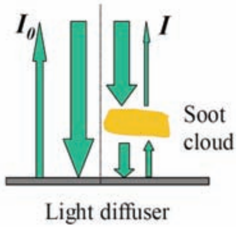

Fig. S-1. Light extinction by the soot cloud.

A variation in the reflected light intensity was caused only by the presence of soot, following the Lambert–Beer Law:

$$I = I_0 \exp(-\int_0^{2L} K_{\text{ext}} \mathrm{d}x) \tag{S-1}$$

where I is the reflected light intensity with or without the presence of a soot cloud, I_0 is the reflected light intensity without the presence of a soot cloud, K_{ext} is the extinction coefficient and L is the path length through the soot cloud. Unlike the traditional back illumination method, the light extinction in the FILE method is proportional to $2L$ rather than L due to the light passing twice through the soot cloud.

The extinction coefficient of the soot cloud is dependent on the particle number density, and on the particle diameter and optical properties. Based on the Rayleigh approximation, the soot volume fraction could be expressed as:

$$C_{\text{v}} = \frac{\lambda}{(2L)K_{\text{a}}} \ln\left(\frac{I_0}{I}\right) \tag{S-2}$$

where λ is the wavelength of mono-wavelength light, K_{a} is the dimensionless absorption constant determined by soot refractive index m. A value of 5.47 was adopted here with $m = 1.62 + i0.66$. The soot volume fraction could be calculated using Eq. (S-2) by analysis of the images with and without soot clouds, pixel by pixel. However, for a non-axisymmetric diesel flame, the thickness of the soot cloud cannot be measured and the only the line-of-sight, expressed as C_vL, can be detected. If the area of each pixel is represented by a dimension of Δr and a mean mass density of soot particles 2.0 g cm^{-1} is adopted,[1] then the soot mass at each pixel could be calculated as:

$$m_i = \rho_s C_v L \Delta r \tag{S-3}$$

Equation (S-3) indicates that each pixel value represented the local soot mass in each column vertical to the image plane, and the total soot mass at this time could be obtained by summing all the pixel values. A detailed introduction about FILE methods in detecting a spray, combustion flame and soot emissions can be found in previous reports.[2-4,5]

DESCRIPTIONS OF THE MODELS

The phenomenological soot model, Fig. 2, has nine main steps: 1) acetylene formed through a fuel pyrolysis process, 2) precursor species formed merely from acetylene pools, 3) soot inception reaction, 4) surface growth of soot nuclei, 5) coagulation of small soot particles to form bigger ones, 6) soot surface oxidation *via* oxygen attachment, 7) soot surface oxidation *via* OH radicals, 8) acetylene oxidized by O_2 and 9) precursor radicals oxidized by OH radicals. All of the reaction formulas, reaction rates and relevant reaction constants are listed in Table S-II. The concentration of OH radical was estimated based on a H_2–O_2–CO_2 system, and a detailed description can be found in a previous study.[6] The precursor species were assumed to be general gaseous soot precursors, such as fullerene, based on the observation of heavier PAHs in hydrocarbon diffusion combustion.[7.8]

TABLE S-II. Reaction mechanism of the phenomenological soot model

No.	Reaction	Reaction rate	$k = A\exp\left(\frac{-E_a}{RT}\right)$	
			A	E_a / kJ mol^{-1}
1	$\text{Fuel} \rightarrow C_2H_2$	$\omega_1 = k_1[\text{Fuel}]$	1.0×10^{10}	207.85
2	$C_2H_2 \rightarrow P_c$	$\omega_2 = k_2[C_2H_2]$	1.0×10^{11}	166.28
3	$P_c \rightarrow S_c$	$\omega_3 = k_3[P_c]$	5.0×10^{7}	209.51
4	$S_c + S_c \rightarrow S_c$	$\omega_4 = k_4N^2$	Collision frequency constant[6]	
5	$S_c + C_2H_2 \rightarrow S_{c+2} + H_2$	$\omega_5 = k_5[C_2H_2]A_s^{\frac{1}{2}}$	1.05×10^{4}	25.77
6	$S_c + O_2 \rightarrow S_{c-2} + 2CO$	$\omega_6 = \frac{6[S_c]MW_c}{\rho_s d_s}k_{NSC}$	NSC Oxygen oxidation model[9]	
7	$S_c + OH \rightarrow S_{c-1} + CO + \frac{1}{2}H_2$	$\omega_7 = \gamma_7\frac{3[OH]}{N_A}\left(\frac{8RT}{\pi M_{OH}}\right)^{\frac{1}{2}}$	The OH oxidation model of Neoh *et al.*[10]	
8	$C_2H_2 + O_2 \rightarrow 2CO + H_2$	$\omega_8 = k_8[C_2H_2][O_2]$	6.0×10^{12}	209.51
9	$P_c + OH \rightarrow CO$	$\omega_9 = k_9[P_c][OH]$	1.0×10^{9}	166.28

In the Tao model,[6] the original principal governing equations for solving the soot mole density and the soot mass density were listed as:

$$\frac{\mathrm{d}[S_\mathrm{c}]}{\mathrm{d}t} = \omega_3 - \omega_4 \tag{S-4}$$

$$\frac{\mathrm{d}m_\mathrm{s}}{\mathrm{d}t} = MW_\mathrm{s}\omega_3 + MW_\mathrm{s}\left(\omega_5 - \omega_6 - \omega_7\right) \tag{S-5}$$

where ω indicates the reaction rate, the subscript number is the number of the reaction listed in Table S-II, MW_s is the molecular weight of the soot particles. Since the flame speed of diffusion combustion is determined by the speed of turbulent mixing, all reaction rates in these equations were modified by the Turbulence-Chemistry interaction model.[11]

Model modification. As can be seen in Eq. (S-4), only inception and coagulation were taken into account for the determination of the soot number density. However, previous results[12] proved that surface oxidation is also possible, which would lead to a reduction in the soot number density. During the early stage of diffusion combustion, the soot formation mechanism dominates the soot evolution and a large number of soot particles in the form of a ball core are newly generated within the chamber. Compressed ignition combustion is a kind of diffusion-controlled combustion, in which the distribution of fuel and oxidants is extremely heterogeneous. Since these young soot particles contain very few carbon atoms, they could be quickly consumed in a locally rich-oxidant environment and finally result in a reduction in soot number density. At a later stage of diffusion combustion, the oxidation mechanism takes the place of the formation mechanism and becomes dominant in soot evolution. Although the mature soot is cluster-like or chain-like hydrocarbon aggregates composed of tens to hundreds of spherical particles, it was still possible for them to be eliminated completely by strong surface oxidation, which would finally lead to a decrease in the soot number quantity. The soot number density is significant for the calculation of the soot mean diameter and the total surface area, which could sequentially affect the final soot mass concentration. Therefore, it is essential to introduce surface oxidation feedback into the calculation of the soot number density.

The effects of surface oxidation on the soot number density were taken into account for both incipient and mature soot particles. For small incipient soot particles, once the surface oxidation wins the competition with surface growth, which means that more carbon atoms were depleted than accumulated on the active surface area, the soot number density began to decrease. For mature soot particles formed after coagulation and surface growth, surface oxidation was required to deplete the shell-shaped surface carbon atoms first before contributing to number density reduction. In order to detect the turning point when surface oxidation began to affect the number density of mature soot particles, a parameter termed as critical diameter, d_cri, was adopted to describe the diameter of an incipient particle and the mean diameter of the soot particle is expressed as:

$$d_\mathrm{s} = \left(\frac{6m_\mathrm{s}}{\pi N_\mathrm{s}\rho_\mathrm{s}}\right)^{1/3} \tag{S-6}$$

where m_s is the soot mass density, N_s is soot number density and ρ_s is the density of the soot particles, which was assumed to be 2 g cm^{-3}.

When surface oxidation loses the competition with surface growth, surface oxidation does not affect the soot number density. The governing differential equation of soot number density is the same as that in the Tao model.[6] When surface oxidation wins the competition with surface growth, but d_s is still larger than d_{cri}, the number density deduction only led to a number density reduction of the incipient soot particles and the adjusted mole density could be represented as:

$$\frac{\mathrm{d}[S_c]}{\mathrm{d}t} = \omega_3 - \omega_4 - \omega_{inc} \tag{S-7}$$

$$\omega_{inc} = \frac{MW_c(\omega_5 - \omega_6 - \omega_7)\omega_3}{MW_s(i)[S_c] + \omega_3 MW_c} \tag{S8}$$

where ω_{inc} is the amount the number density of incipient soot particles is reduced because of oxidation effects. When surface oxidation wins the competition with the surface growth and simultaneously d_s is equal or less than d_{cri}, number density reduction occurs in both incipient and mature soot particles and the revised soot mole density can be represented as:

$$\frac{\mathrm{d}[S_c]}{\mathrm{d}t} = \omega_3 - \omega_4 + \frac{MW_c}{MW_s(i)}(\omega_5 - \omega_6 - \omega_7) \tag{S-9}$$

where $MW_s(i)$ is the mean molecular weight of soot particles of computational cells i (i denotes the cell number). As soot is a super complex aggregate, in the present study, $MW_s(i)$ was not considered a constant as previously,[6] but was renewed after each computational time step.

Numerical implementation. In this study, KIVA-3V Release 2 code was the numerical solver to calculate the mass, momentum and energy conservation equations for soot and other gas-phase species involved in the diesel combustion system. Spray dynamics was simulated using the "blob" injection model.[13] Spray atomization and droplet breakup were modeled by the Rayleigh–Taylor model.[14] The RNG k–ε model[15] for turbulent flow was also included to interpret the average effects of turbulent motions on the main flow characteristics, such as mass, density, velocity, *etc*. The ignition was modeled using the Shell ignition model.[16]

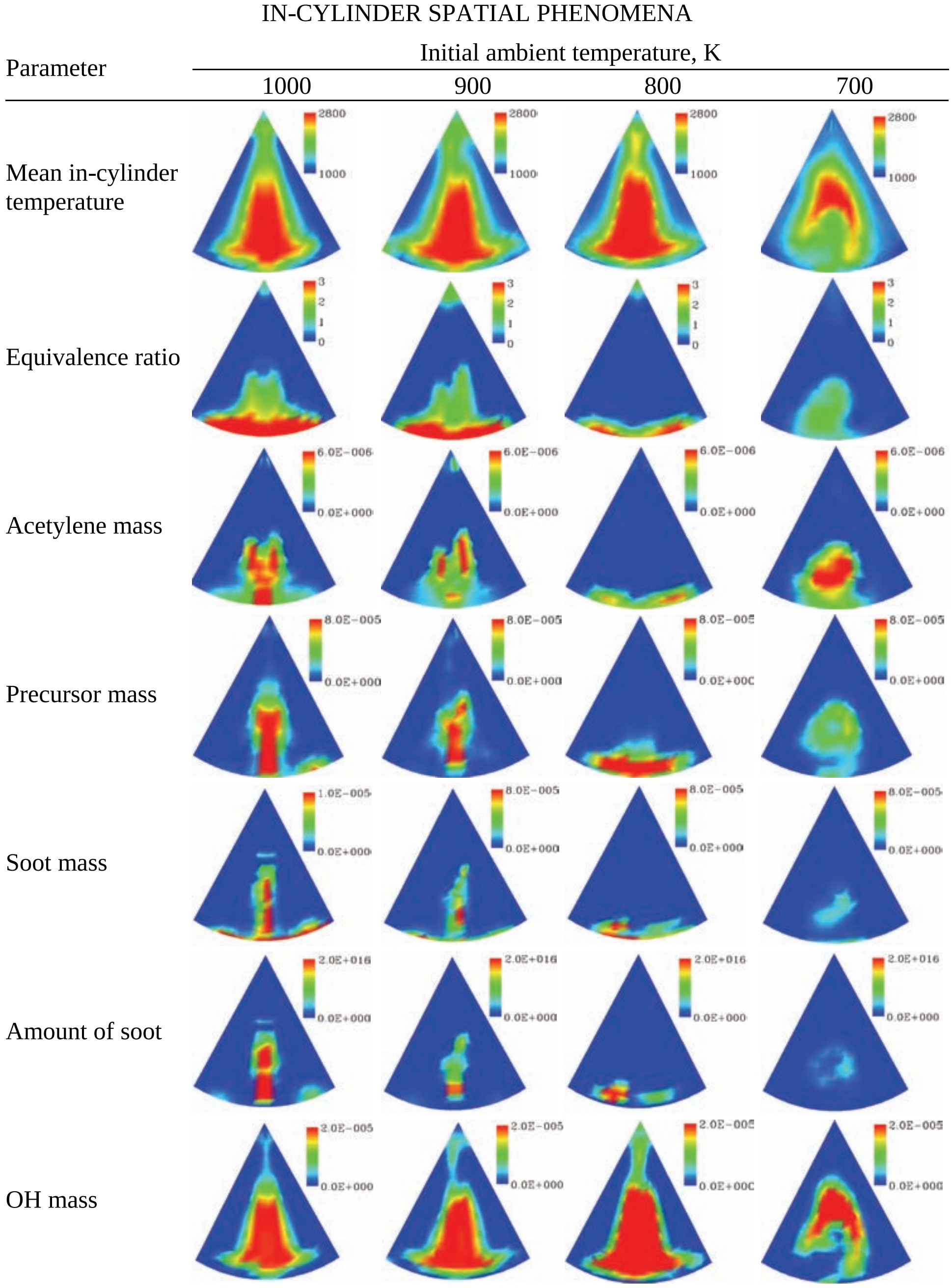

Fig. S-2. Spatial distributions of the in-cylinder temperature, mass of acetylene, precursor species, soot nuclei, OH radicals and amount of soot generated in 4.5 ms by 1 g fuel for ambient temperatures of 700, 800, 900 and 1000 K. The bars on the upper right corners present the upper and lower limits for each parameter.

NOMENCLATURE

A	Exponential factor
A_s	Surface area of soot particle
C_v	soot volume fraction
d_cri	Critical diameter of incipient soot particles
d_s	Diameter of soot particle
E_a	Activation energy
FILE	Illumination light extinction
i	Cell number
I	Reflected light intensity
I_0	Reflected light intensity without the presence of a soot cloud
K_a	Dimensionless absorption constant
K_ext	Extinction coefficient
L	Path length through the soot cloud
m	Soot refractive index
m_s	Soot mass concentration
MW_c	Molar weight of carbon atom
MW_s	Molar weight of soot particle
MW_OH	Molar weight of OH radical
N_s	Number density of soot particle
N_A	Avogadro’s number
NSC	Nagle–Stickland–Constable oxidation model
p	Mean pressure
$[\mathrm{P_c}]$	Mole concentration of soot precursor
R	Universal gas constant
Δr	Area of each pixel
$[S_\mathrm{c}]$	Mole concentration of soot particle
T	Mean temperature
λ	Wavelength of monochromic light
ρ_s	Soot particle density
ω	Reaction rate
ω_mc	Reduced incipient soot number density caused by the oxidation effects

REFERENCES

1. A. Braun, F. E. Huggins, S. Seifert, J. Ilavsky, N. Shah, K. E. Kelly, A. Sarofim, G. P. Huffman, Combust. Flame 137 (2004) 63
2. H. Liu, X. Bi, M. Huo, C. F. F. Lee, M. Yao, Energy Fuels 26 (2012) 1900
3. H. Liu, C. F. Lee, M. Huo, M. Yao, Energy Fuels 25 (2011) 1837
4. H. Liu, C. F. F. Lee, M. Huo, M. Yao, Energy Fuels 25 (2011) 3192
5. Y. Xu, C. F. Lee, Appl. Optics 45 (2006) 2046
6. F. Tao, R. D. Reitz, D. E. Foster, Y. Liu, Int. J. Therm. Sci. 48 (2009) 1223
7. A. Keller, R. Kovacs, K. H. Homann, Phys. Chem. Chem. Phys. 2 (2000) 1667
8. O. Mathieu, G. Frache, N. Djebaïli-Chaumeix, C. E. Paillard, G. Krier, J. F. Muller, F. Douce, P. Manuelli, Proc. Combust. Inst. 31 (2007) 511
9. H. Hiroyasu, T. Kadota, M. Arai, B. JSME 26(1983) 569.
10. K. G. Neoh, J. B. Howard, A. F. Sarofim, Proc. Combust. Inst. 20 (1985) 951
11. L. A. Vulis, T. P. Leontéva, Z. B. Sakipov, I. B. Palatnik, B. P. Ustimenko, Int. J. Heat Mass Tran. 4 (1961) 111

12. D. R. Tree, K. I. Svensson, Prog. Energ. Combust. Sci. 33 (2007) 272
13. R. D. Reitz, R. Diwakar, Structure of High-Pressure Fuel Sprays, SAE Technical Paper 870598, 1987, doi: 10.4271/870598
14. M. Patterson, S. Kong, G. Hampson, R. D. Reitz, Modeling the Effects of Fuel Injection Characteristics on Diesel Engine Soot and NOx Emissions, SAE Technical Paper 940523, 1994, doi: 10.4271/940523
15. Z. Han, R. D. Reitz, Combust. Sci. Technol. 31 (1995) 267
16. S. Kong, Z. Han, R. D. Reitz, The Development and Application of a Diesel Ignition and Combustion Model for Multidimensional Engine Simulation, SAE Technical Paper 950278, 1995, doi: 10.4271/950278.